Paper No.
08395

NACE INTERNATIONAL CORROSION 2008 CONFERENCE & EXPO

A METHOD TO REDUCE THE INTERNAL CURRENT EFFECT ON LOCALIZED CORROSION MEASUREMENTS WITH COUPLED MULTIELECTRODE ARRAY SENSORS

Lietai Yang and Xiaodong Sun
Corr Instruments, LLC
San Antonio, TX 78226

ABSTRACT

Coupled multielectrode array sensors (CMAS) have been extensively used to measure localized corrosion rate in laboratories and plants. A convenient way to calculate localized corrosion rate is to assume that the internal current flow within the most anodic electrode is insignificant. In cases where the environment is not significantly corrosive, this assumption may not be true. The internal electron that flows on the most corroding electrode may cause the CMAS to underestimate the non-uniform corrosion rates. A new method has been derived to minimize the internal currents within the most anodic electrode. This paper describes the method and presents some experimental results.

Keywords: Multielectrode sensor, multielectrode probe, corrosion monitoring, corrosion sensor, localized corrosion sensor, online corrosion sensor, real-time corrosion sensor, coupled multiple electrodes.

INTRODUCTION

The concept of coupled multielectrode is one of the new developments in the past decade in the measurements of corrosion behaviors and studies of spatiotemporal patterns of electrochemical processes on metal surfaces.[1-7] Coupled multielectrode array sensors (CMASs) give direct, one-parameter non-uniform corrosion rates derived from statistical parameters such as standard deviation of currents or most anodic current from the multiple electrodes[8,9]. These probes have made the quantitative real-time and online monitoring of non-uniform corrosion, especially localized corrosion such as pitting and crevice corrosion possible. The CMAS technology has been used successfully for online and real-time monitoring of corrosion in many different laboratories and industrial fields.[8-48]

A simple and convenient way to determine the quantitative penetration rate of localized corrosion using a CMAS probe involves the assumption that there is no current that flows internally on the most corroding electrode.[10] This is a reasonable assumption if the metal is not corrosion resistant or if the environment is highly corrosive. In these cases, a high probability exists that at least one or two of the probe electrodes corrode severely. Under these conditions, no cathodic site is likely to exist on the

most severely corroding electrode of the probe to accept electrons from the corroding sites on the same electrode.[48] However, for a corrosion resistant alloy in a less corrosive environment, or for a metal in a corrosive environment during the early stages of corrosion when no electrode is more significantly corroded than the others in the probe, the assumption of zero internal current may underestimate the true localized corrosion penetration rate. This paper describes a new method that may be used to reduce the internal current on the most corroding electrode and thus reduce the uncertainty that may be caused by the internal current.

PRINCIPLE

Figure 1 shows typical CMAS probes for laboratory and industrial field applications.[9,32] Figure 2 shows the working principle of the CMAS probes.[9, 32, 48] The most anodic current*, the current that flows through the external circuit from the most corroding electrode (or most anodic electrode) to the less corroding or non-corroding electrodes (cathodic electrodes) is usually used to derive the localized corrosion rate. The anodic current on the most corroding electrode corresponds to the highest corrosion rate or maximum penetration rate on a probe that simulates a metal coupon. Thus the corrosion rate from a CMAS probe represents the highest penetration rate of localized corrosion (e.g., pitting corrosion) that may be found on a metal coupon.

Figure 3 shows the schematic diagram for the polarization curves of the most anodic electrode (the most corroding electrode in Figure 2) and several other cathodic electrodes that support the anodic reactions on the most anodic electrode. The thin curves represent the dissolution and reduction polarization behaviors on the most anodic electrode. The thick curves represent the combined dissolution and reduction polarization behaviors on the several cathodic electrodes if these cathodic electrodes are coupled as a single electrode. Note, these or some of these cathodic electrodes may also support the anodic reactions taking place on the other anodic electrodes of the probe, but only the portion of currents that is required to balance the anodic current from the most anodic electrode is represented in the polarization curves for cathodic electrode. For a passive metal, in the cathodic area (or the cathodic electrodes in a CMAS probe) where no localized corrosion has been initiated, the anodic current is usually extremely low due to the protective layer of the oxide formed on the metal and the corrosion potential for the cathodic electrodes, E^c_{corr}, is high (or noble).[49-50] For the most anodic electrode where localized corrosion has been initiated and the protective layer has been compromised, however, the anodic current is usually high and the corrosion potential for the anodic electrode, E^a_{corr}, is low (or active). Note in Figure 3, the cathodic current on the combined cathodic electrodes is significantly higher than that on the most anodic electrode. This is because the most anodic electrode is fully covered by corrosion products (Figure 2) and the cathodic reactions that would take place deep in the pit on the most anodic electrode require more efforts for the reactants (O_2 or H^+) to overcome the mass transfer barrier. In addition, the surface area on the most anodic electrode is smaller than that of the cathodic electrodes because one anodic electrode is supported by many cathodic electrodes.

When the most anodic electrode and the combined cathodic electrodes are coupled, the corrosion potential changes to a new value, E_{coup} (or E_{corr} for all coupled electrodes), and the total anodic dissolution currents equal the total cathodic reduction currents:

$$|I_{corr}| + |I^c_{in}| = |I^a_{in}| + |I^c| \quad (1)$$

Where I_{corr} is the corrosion current (total dissolution current) on the most anodic electrode, I^c_{in} is the dissolution (anodic) current on all the cathodic electrodes (anodic current that flows within all the

* The statistical equivalents of the most anodic current, such as the value of mean current plus 2.5 or 3 times the standard deviation of the currents from the different electrodes or the value of the 95th percentile of anodic currents from the different electrodes were also used[10]. To simplify the discussion, this paper will focus on the use of the most anodic current to derive the corrosion rate.

cathodes), I^a_{in} is the reduction current on the most anodic electrode (the cathodic current that flows within the most anodic electrode), and I^c the cathodic current on the combined cathodic electrodes.

On the most anodic electrode, the corrosion current (total dissolution current), I_{corr}, is equal to the sum of the externally flowing anodic current, I_{ex}, and the internally flowing anodic current which is equal to the reduction current, I^a_{in}. Therefore,

$$I_{corr} = I_{ex} + |I^a_{in}| \quad (2)$$

For the case shown in Figures 2 and 3, the I^a_{in} for the most anodic electrode of the CMAS probe is much smaller than its I_{ex} at the coupling potential in a localized corrosion environment, the externally flowing current from such an anodic electrode of the probe can often be directly used to estimate the localized corrosion current:

$$I_{corr} \approx I_{ex} \quad (3)$$

Figure 4 shows a case where localized corrosion is not significant. The most anodic electrode still has significant cathodic sites available, and some electrons from the anodic sites flow internally to the cathodic sites within the same electrode. The corresponding schematic diagram for the polarization curves of the most anodic electrode and several other cathodic electrodes that support the anodic reactions on the most anodic electrode is shown in Figure 5. Unlike Figure 3, the I^a_{in} in Figure 5 is significant and cannot be ignored in the calculation for the corrosion current. In this case, Equation (2) may be represented as:[9,10]

$$I_{ex} = \varepsilon I_{corr} \quad (4)$$

where ε is a current distribution factor that represents the fraction of electrons resulting from corrosion that flow through the external circuit. The value of ε may vary between 0 and 1, depending on parameters such as surface heterogeneities on the metal, the environment, the electrode size, and the number of sensing electrodes. If the most corroding electrode is severely corroded and significantly more anodic than the other electrodes in the probe, the ε value for this corroding electrode would be close to 1 ($I^a_{in} = 0$), and the measured external current would be equal to the localized corrosion current [Equation (3)].[10]

Because the value of ε varies, there are uncertainties in the corrosion rate if Equation (4) is used to calculate the corrosion rate. To reduce this uncertainty, a method was proposed to force all the electrons produced on the most corroding electrode to flow externally, and thus to make ε=1.[25] This was achieved by applying an external power source to raise the potential of the coupling joint of the multielectrode sensor probe, such that the current from the most cathodic electrode would be close to zero. In this way, the coupling joint of the sensor is statistically at the highest potential of all reaction sites of the metal, if the sites can be separated from each other. At such a potential, no cathodic sites would be statistically available on the most anodic electrode to receive the electrons produced on the same corroding electrode. [25]

NEW APPROACH

The above mentioned potential-perturbation method requires an external power source and an additional counter electrode to polarize the coupling joint of the CMAS probe. This paper presents an alternative method for raising the coupling potential by using the cathodic electrodes of the CMAS probe, with no additional power source. When the current from the most corroding electrode of a CMAS probe is used to derive the maximum localized corrosion rate, the currents from the other anodic electrodes are not used.[9] These less anodic electrodes can be disconnected from the coupling joint so that all the cathodic electrodes would only support the anodic reactions on the single most anodic

electrode (Figure 6). The corresponding schematic diagram for the polarization curves of the most anodic electrode and the other cathodic electrodes that support the most corroding electrode is shown in Figure 7. Because all the cathodic electrode are supporting only one anodic electrode, the cathodic current (the thick line) are now relatively higher than in Figure 5 and the coupling potential is raised to E'_{coup}. At this new coupling potential, the value of the internal anodic current on the most anodic electrode of the CMAS probe, $I^{a'}_{in}$, is close to zero and the corrosion current, I'_{Corr}, in Equations (2) or (4) is close to the externally measured coupling current, I'_{ex} (i.e., $I'_{Corr} \approx I'_{ex}$).

EXAMPLE RESULTS

An experiment was conducted to verify the new approach. A modified S-50 coupled multielectrode array sensor analyzer and the associated software by Corr Instruments (San Antonio, TX) were used to measure the localized corrosion rate of a CMAS probe made of 14 low carbon steel electrodes. The electrodes were flush-mounted and each electrode had a surface area of 0.065 cm^2. The modified CMAS analyzer has additional switches that can be used to connect or disconnect any of the electrodes of the CMAS probe to or from the coupling joint. The test solution was air-saturated simulated seawater (0.5 M NaCl).

Figure 8 shows the current from each electrode of the probe immersed in the simulated seawater, both with and without disconnecting (decoupling) the less anodic electrodes. When the less anodic electrodes were disconnected from the coupling joint, the anodic currents that were required to support the cathodic reactions at the cathodic electrodes were provided mainly by the most corroding electrode (Electrode #10 or Electrode #1). Therefore, its current increased approximately by 2 to 3 times. Because the decoupling of the other anodic electrodes would cause the corrosion potential of the CMAS probe to shift positively (Figure 7), most of the electrons produced on the most anodic electrode are expected to flow externally ($I^{a'}_{in}$ in Figure 7 close to zero). The increases in the anodic current from the most anodic electrode after the decoupling of the less anodic electrodes verified the concept of the decoupling approach.

The slight polarization of the most anodic electrode in the anodic direction may also initiate corrosion at the sites that would otherwise not have any corrosion. Therefore, the decoupling of some of the anodic electrodes may give a higher corrosion rate than the true corrosion rate on the most corroding electrode that remains connected to the coupling joint. The anodic current measured under this condition would be a bounding localized corrosion current for the metal under the given environment. This is because some of the localized corrosion sites (pits for example) may be surrounded by a very large uncorroded cathodic area. This bounding current can be used to determine the bounding maximum localized corrosion rate. Figure 9 shows the comparison between the localized corrosion rate obtained from the most corroding electrode without decoupling the less anodic electrodes, r_{max}, and the localized corrosion rate obtained from the most corroding electrode with decoupling the less anodic electrodes, r'_{max}.

CONCLUSIONS

A method for measuring bounding localized corrosion rate using coupled multielectrode array sensor probes was discussed. The bounding localized corrosion rate is measured from the most corroding electrode after disconnecting the less anodic electrodes of the probe from the coupling joint. The decoupling of the less anodic electrode causes the increase in the coupling potential because fewer numbers of the anodes are supported by the cathodic electrodes that have high open-circuit potentials. The increase in the coupling potential leads to the reduction or elimination of the internally flowing electrons on the most corroding electrode. Thus, the externally measured anodic current equals the corrosion current on the most corroding electrode. Experimental results that support the decoupling concept were presented.

REFERENCES

1. U. Steinsmo, T. Rone, and J.M. Drugli, “Aspects of Testing and Selecting Stainless Steels for Sea Water Applications,” CORROSION/94, paper no. 492, Houston, TX: NACE, 1994.

2. Z. Fei, R.G. Kelly, and J.L. Hudson, Journal of Physical Chemistry, 100(49), pp. 18,986-18,991, 1996.

3. Y.J. Tan, Corrosion Science, 41(2), pp. 229-247, 1999.

4. Y. J. Tan, T. Liu and N. Aung, “Localized Corrosion and Inhibition Studies Using the Wire Beam Electrode Method in Conjunction with the Electrochemical Noise Analysis and the Scanning Reference Electrode Technique,” CORROSION/2004, paper no. 04427, Houston, TX: NACE, 2004.

5. N.D. Budiansky, J.L. Hudson, J.R. Scully, “Origins of Persistent Interaction among Localized Corrosion Sites on Stainless Steel,” Journal of the Electrochemical Society (2004), 151(4), B233-B243].

6. H. Cong, N. D. Budiansky and J. R. Scully, H. T. Michels, “Use of Coupled Electrode Arrays to Elucidate Copper Pitting as a Function of Potable Water Chemistry” CORROSION/07, paper no. 07392, Houston, TX: NACE, 2007.

7. F.D. Wall, and M.A. Martinez, “A Statistics-Based Approach to Studying Aluminum Pit Initiation — Intrinsic and Defect-Driven Pit Initiation Phenomena,” Journal of the Electrochemical Society, 2003. 150(4): p. B146-B157.

8. L. Yang and N. Sridhar, “Monitoring of Localized Corrosion”, in ASM Handbook, Volume 13A-Corroson:Fundmentals, Testing, and Protection, Stephen. D. Crammer and Bernard S. Covino, Jr., eds, Materials Park, OH: ASM , pp. 519-524, 2003.

9 L. Yang and N. Sridhar, Materials Performance, 42(9), pp. 48-52, 2003.

10. L. Yang, N. Sridhar, O. Pensado, and D. S. Dunn, Corrosion, 58, p. 1,004, 2002.

11 L. Yang, and D. S. Dunn, “Evaluation of Corrosion Inhibitors in Cooling Water Systems Using a Coupled Multielectrode Array Sensor,” CORROSION/2002, paper no. 02004, Houston, TX: NACE, 2002.

12 L. Yang, N. Sridhar, and G. Cragnolino, “Comparison of Localized Corrosion of Fe-Ni-Cr-Mo Alloys in Concentrated Brine Solutions Using a Coupled Multielectrode Array Sensor,” NACE Corrosion/2002, paper no. 545, NACE, 2002.

13 C. Sean Brossia and Lietai Yang, “Studies of Microbiologically Influenced Corrosion Using a Coupled Multielectrode Array Sensor,” CORROSION/2003, paper no. 03575, Houston, TX: NACE International, 2003.

14 V. Jain, S. Brossia, D. Dunn, and L. Yang, “Development of Sensors for Waste Package Testing and Monitoring in the Long Term Repository Environments,” Ceramic Transactions Vol. 143, Westerville, OH: American Ceramic Society, pp. 283-290, 2003.

15 L. Yang, R.T. Pabalan, L. Browning, and D.S. Dunn, “Corrosion Behavior of Carbon Steel and Stainless Steel Materials Under Salt Deposits in Simulated Dry Repository Environments,”

Scientific Basis for Nuclear Waste Management XXVI, Symposium Proceedings 757R, J. Finch and D. B. Bullen, eds, Warrendale, PA: Materials Research Society, pp. 791-797, 2003.

16 L. Yang, R. T. Pabalan, L. Browning, and G. A. Cragnolino, "Measurement of Corrosion in Saturated Solutions Under Salt Deposits Using Coupled Multielectrode Array Sensors," CORROSION/2003, paper no. 03426, Houston, TX: NACE, 2003.

17 A. Anderko, N. Sridhar, C. S. Brossia, D. S. Dunn, L.T. Yang, B.J. Saldanha, S.L. Grise, and M.H. Dorsey, "An Electrochemical Approach to Predicting and Monitoring Localized Corrosion in Chemical Process Streams," CORROSION/2003, paper no. 03375, Houston, TX: NACE, 2003.

18. M. H. Dorsey, L. Yang and N. Sridhar, "Cooling Water Monitoring Using Coupled Multielectrode Array Sensors and Other On-line Tools," CORROSION/2004, paper no. 04077, Houston, TX: NACE, 2004.

19. L. Yang, N. Sridhar, S.L. Grise, B.J. Saldanha, M.H. Dorsey, H.J. Shore, and A. Smith, "Real-Time Corrosion Monitoring in a Process Stream of a Chemical Plant Using Coupled Multielectrode Array Sensors," CORROSION/2004, paper no. 04440, Houston, TX: NACE, 2004.

20. L. Yang, N. Sridhar, D.S. Dunn, and C.S. Brossia, "Laboratory Comparison of Coupled Multielectrode Array Sensors with Electrochemical Noise Sensors for Real-Time Corrosion Monitoring," CORROSION/2004, paper no. 04033, Houston, TX: NACE, 2004.

21. X. Sun, "Online Monitoring of Undercoating Corrosions Utilizing Coupled Multielectrode Sensors," CORROSION/2004, paper no. 04033, Houston, TX: NACE, 2004.

22. X. Sun, "Online Monitoring of Corrosion under Cathodic Protection Conditions Utilizing Coupled Multielectrode Sensors," CORROSION/2004, paper no. 04094, Houston, TX: NACE, 2004.

23 L. Yang and G. A. Cragnolino, "Studies on The Corrosion Behavior of Stainless Steels in Chloride Solutions in the Presence of Sulfate Reducing Bacteria," CORROSION/2004, paper no. 04598, Houston, TX: NACE, 2004.

24. L. Yang and N. Sridhar, "Sensor Array and Method for Electrochemical Corrosion Monitoring," U.S. Patent No. 6,683,463 (2004).

25. L. Yang, D. S. Dun and G. A. Cragnolino, "An Improved Method for Real-time and Online Corrosion Monitoring Using Coupled Multielectrode Array Sensors," CORROSION/2005, paper no. 05379, Houston, TX: NACE, 2005.

26. L. Yang and N. Sridhar, "Coupled Multielectrode Array Systems and Sensors for Real-Time Corrosion Monitoring - A Review," CORROSION/2006, paper no. 06681, Houston, TX: NACE, 2006.

27 L. Yang, N. Sridhar, C. S. Brossia and D. S. Dunn, "Evaluation of the Coupled Multielectrode Array Sensor as a Real Time Corrosion Monitor", Corrosion Science, Vol 47, pp.-1794-1809 (2005).

28. A. Anderko, N. Sridhar1 and L. Yang, S.L. Grise, B.J. Saldanha, and M.H. Dorsey, "Validation of a Localized Corrosion Model Using Real-Time Corrosion Monitoring in a Chemical Plant," Corrosion Engineering, Science and Technology (formerly British Corrosion J.), Vol 40, pp.33-42, August, 2005.

29. L. Yang, D. Dun, Y.-M. Pan and N. Sridhar, “Real-time Monitoring of Carbon Steel Corrosion in Crude Oil and Brine Mixtures Using Coupled Multielectrode Sensors” CORROSION/2005, paper no. 05293, Houston, TX: NACE, 2005.

30. M. H. Dorsey, D. R. Demarco, B. J. Saldanha, G. A. Fisher, L. Yang and N. Sridhar, “Laboratory Evaluation of a Multi-Array Sensor for Detection of Underdeposit Corrosion and/or Microbially Influenced Corrosion,” CORROSION/2005, paper no. 05371, Houston, TX: NACE, 2005.

31. X. Sun and L. Yang, “Real-time Measurement of Crevice Corrosion with Coupled Multielectrode Array Sensors,” CORROSION/2006, paper no. 06679 Houston, TX: NACE, 2006.

32. X. Sun and L. Yang, “Real-Time Monitoring of Localized and General Corrosion Rates in Simulated Marine Environments Using Coupled Multielectrode Array Sensors,” CORROSION/2006, paper no. 06284, Houston, TX: NACE, 2006.

33. X. Sun and L. Yang, ”Real-Time Monitoring of Localized and General Corrosion Rates in Drinking Water Utilizing Coupled Multielectrode Array Sensors,” CORROSION/2006, paper no. 06094, Houston, TX: NACE, 2006.

34. K. T. Chiang and L. Yang, “Monitoring Corrosion Behavior of a Cu-Cr-Nb Alloy by Multielectrode Sensors,” CORROSION/2006, paper no. 06676, Houston, TX: NACE, 2006.

35. N. Sridhar, L. Yang and F. Song, “Application of Multielectrode Array to Study Dewpoint Corrosion in High Pressure Natural Gas Pipeline Environments,” CORROSION/2006, paper no. 06673, Houston, TX: NACE, 2006.

36. X. Sun, "Online and Real-Time Monitoring of Carbon Steel Corrosion in Concrete, Using Coupled Multielectrode Sensors", CORROSION/2005, paper no.05267, Houston, TX: NACE, 2005.

37. X. Sun, “Real-Time Corrosion Monitoring in Soil with Coupled Multielectrode Sensors,” CORROSION/2005, paper no.05381, Houston, TX: NACE, 2005.

38. X. Sun, "Online Monitoring of Undercoating Corrosion Using Coupled Multielectrode Sensors," Materials Performance, 44(2), p28-32 (2005).

39. P. Angell, “Use of the Multiple-Array-Sensor to Determine the Effect of Environmental Parameters on Microbial Activity and Corrosion Rates,” CORROSION/2006, paper no. 06671, Houston, TX: NACE, 2006.

40. L. Yang and N. Sridhar, “Sensor Array for Electrochemical Corrosion Monitoring,” US Patent, #6,987,396 (United States Patent and Trademark Office, 2006).

41. X. Sun Yang, “Electronic system for multielectrode sensors and electrochemical devices.” US Patent, #7,180,309 (United States Patent and Trademark Office, 2007).

42. B. Yang, F.J., Marinho, A.V. Gershun, “New Electrochemical Methods for the Evaluation of Localized Corrosion in Engine Coolants,” Journal of ASTM, Volume 4, Issue 1 (2007),

43. T. Pickthall, V. Morris, and H. Gonzalez, “Corrosion Monitoring of a Crude Oil Pipeline A Comparison of Multiple Methods,” CORROSION/07, paper no. 07340, Houston, TX: NACE, 2007.

44. L. Yang and X. Sun, “Measurement of Cumulative Localized Corrosion Rate Using Coupled Multielectrode Array Sensors,” CORROSION/2007, paper no. 07378, Houston, TX: NACE, 2007.

45. K.T. Chiang and Lietai Yang, “Development of Crevice-Free Multielectrode Sensors for Elevated Temperature Applications,” CORROSION/2007, paper no. 07376, Houston, TX: NACE, 2007.

46. D. Duke, L. Yang, “Laboratory and Field Studies of Localized and General Corrosion Inhibiting Behaviors of Silica in Zero Liquid Discharge (High TDS Cooling Water) using Real Time Corrosion Monitoring Techniques,” CORROSION/2007, paper no. 07626 (Houston, TX: NACE, 2007).

47. Garth Tormoen, James Dante, and Narasi Sridhar, “Correlation of In-Situ VCI Adsorption Monitoring with Real-Time Corrosion Rate Measurements”, CORROSION/2007, paper no. 07356, Houston, TX: NACE, 2007.

48. L. Yang and K.T. Chiang, “A review of Coupled Multielectrode Array Sensors for Corrosion Monitoring and Studies on the Behaviors of the Anodic and Cathodic Electrodes,” Submitted to Journal of ASTM, 2007.

49. N. Sridhar, D.S. Dunn, C.S. Brossia and G.A. Cragnolino, “Stabilization and Repassivation of Localized Corrosion,” in Localized Corrosion, Research Topical Symposium, G.S. Frankel and J.R. Scully, eds, Houston, TX: NACE, pp. 1 29, 2001.

50. H. Boehni and F. Hunkeler, “Growth Kinetics and Stability of Localized Corrosion Processes,” in Advances in Localized Corrosion, H.S. Isaacs, U. Bertocci, J. Kuger, and S. Smialowska, eds, Houston, TX: NACE, p. 69, 1990.

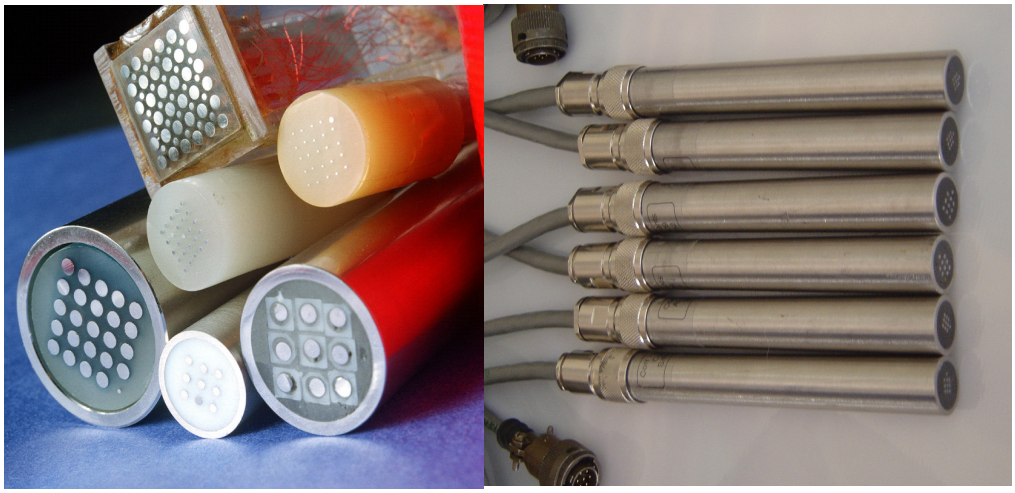

FIGURE 1. Typical CMAS probes for laboratory and industrial field applications.[9,32]

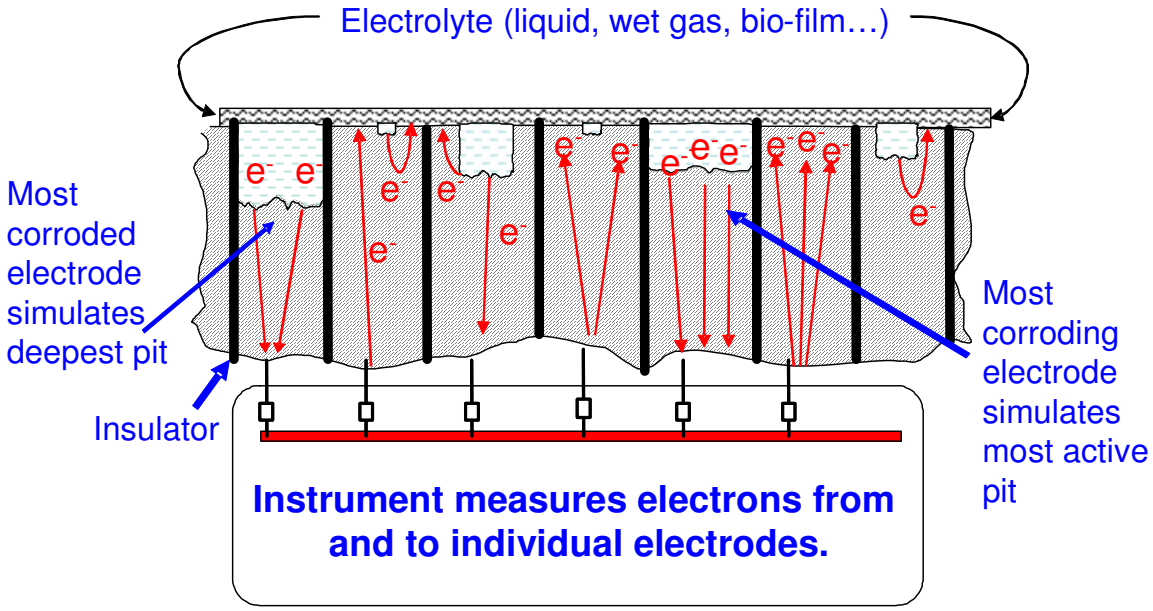

FIGURE 2. Flow of electrons on the different electrodes of a CMAS probe that simulates the corrosion of a metal under a corrosive electrolyte (liquid, salt deposits, or a condensate layer formed in a humid gas) for a case where all the electrons from the most corroding electrode flow externally to the other electrodes.

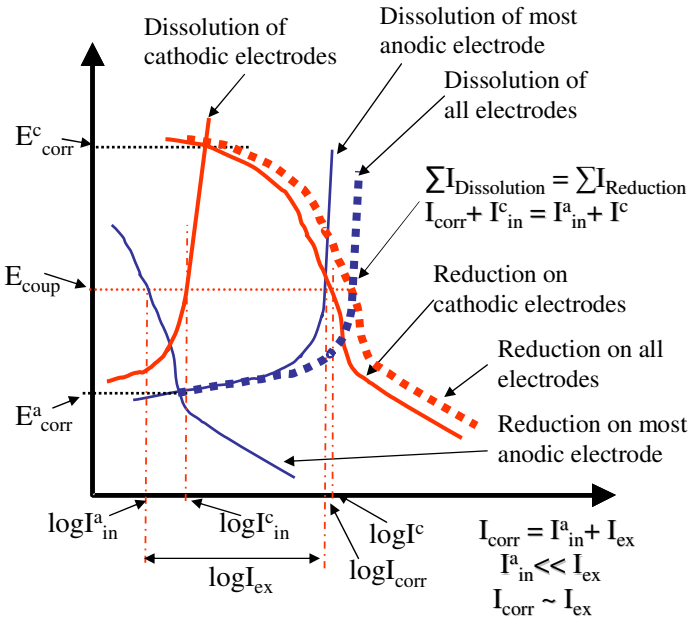

FIGURE 3. Schematic diagram for the polarization curves of the most anodic electrode and the cathodic electrodes that support the anodic dissolution reactions on the most anodic electrode for the case corresponding to Figure 2.

Note: The currents shown in the figure for the cathodic electrodes only include the portion that is required to support the anodic reactions on the most anodic electrodes.

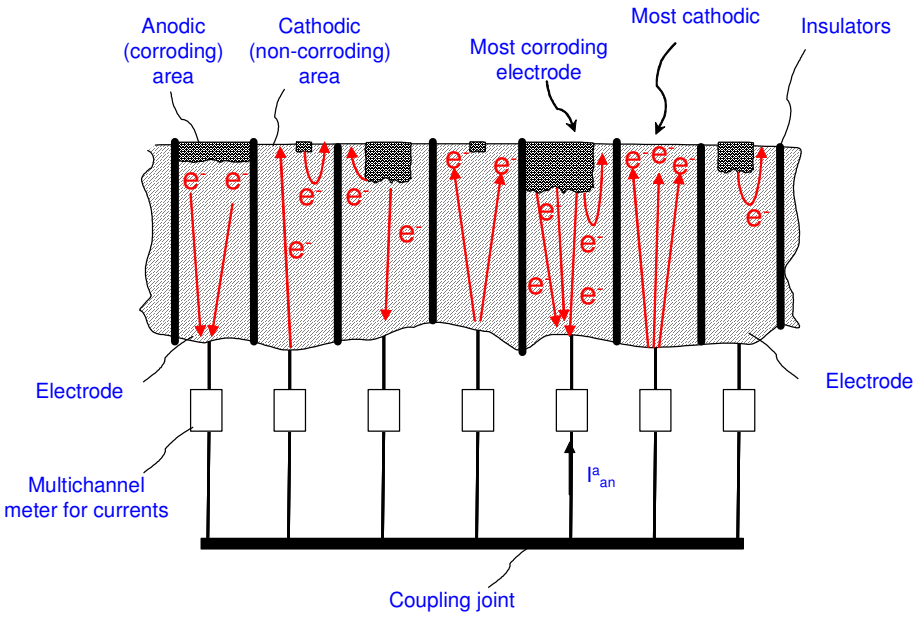

FIGURE 4. Schematic diagram showing a case where the most corroding electrode still has cathodic sites available and some electrons from the anodic sites on the most corroding electrode flow internally to the cathodic sites within the same electrode.

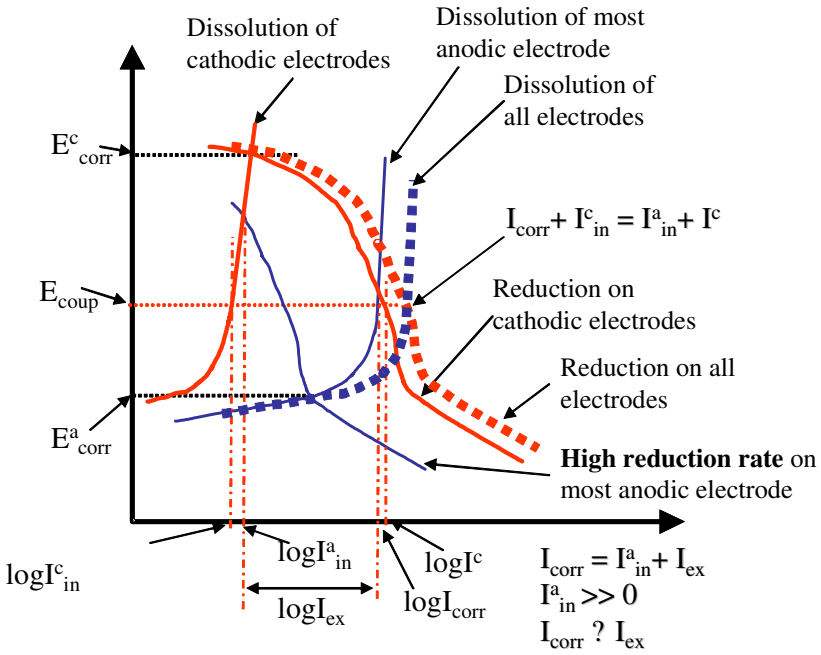

FIGURE 5. Schematic diagram for the polarization curves of the most corroding electrode and the cathodic electrodes that support the anodic dissolution reactions on the most anodic electrode for the case corresponding to Figure 4 where high cathodic current is present on the most anodic electrode.

Note: The currents shown in the figure for the cathodic electrodes only include the portion that is required to support the anodic reactions on the most anodic electrodes.

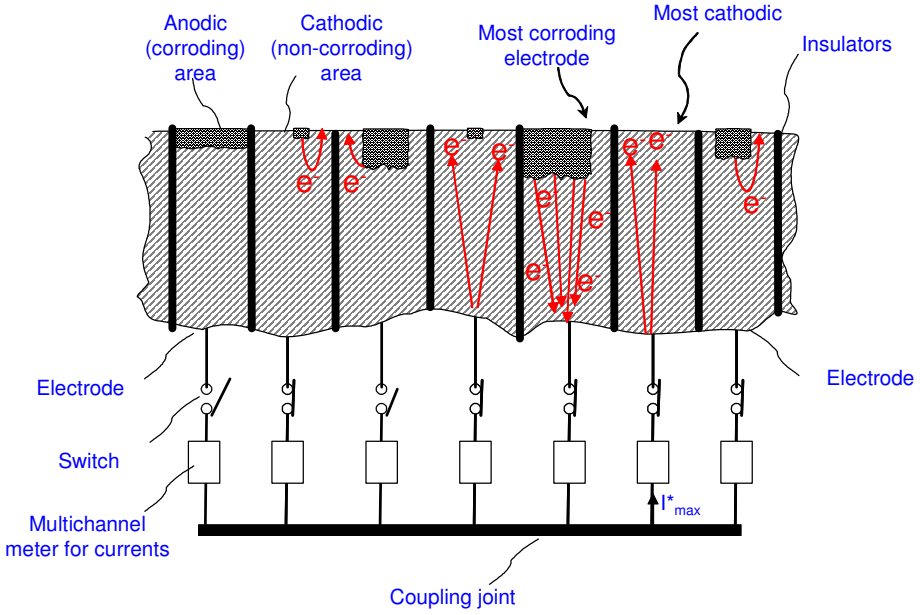

FIGURE 6. Schematic diagram showing that all electrons on the most corroding electrode flow externally to the other electrode after the less anodic electrodes are disconnected from the coupling joint. There is no electron flowing internally on the most corroding electrode.

Patent pending.

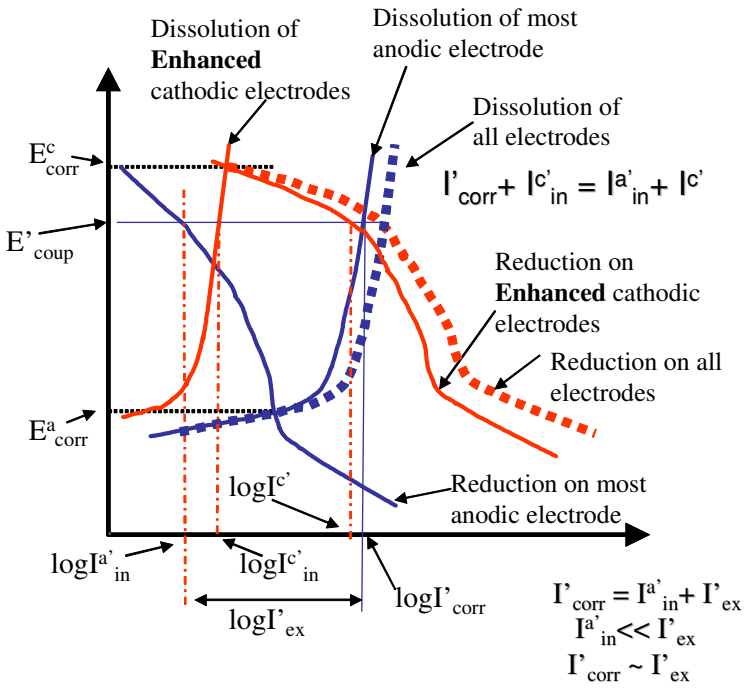

FIGURE 7. Schematic diagram for the polarization curves of the most corroding electrode and the cathodic electrodes that support the anodic dissolution reactions on the most anodic electrode for the case corresponding to Figure 6 where high cathodic current is present on the most corroding electrode and more cathodes are forced to support the anodic reactions on the most corroding electrode.

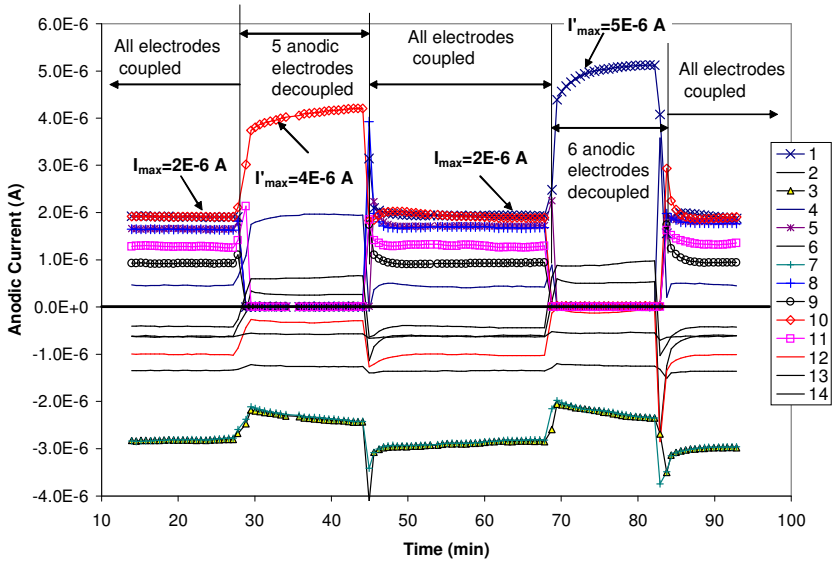

FIGURE 8. Responses of the currents from a 14-electrode CMAS probe made of carbon steel in a 0.5 M NaCl solution to the decoupling of the less anodic electrodes.
Note: The numbers in the legend are the identification numbers of the electrodes in the probe. Electrodes #10 and #1 were the most corroding electrodes at time 20 and time 65 minutes, respectively.

Patent pending.

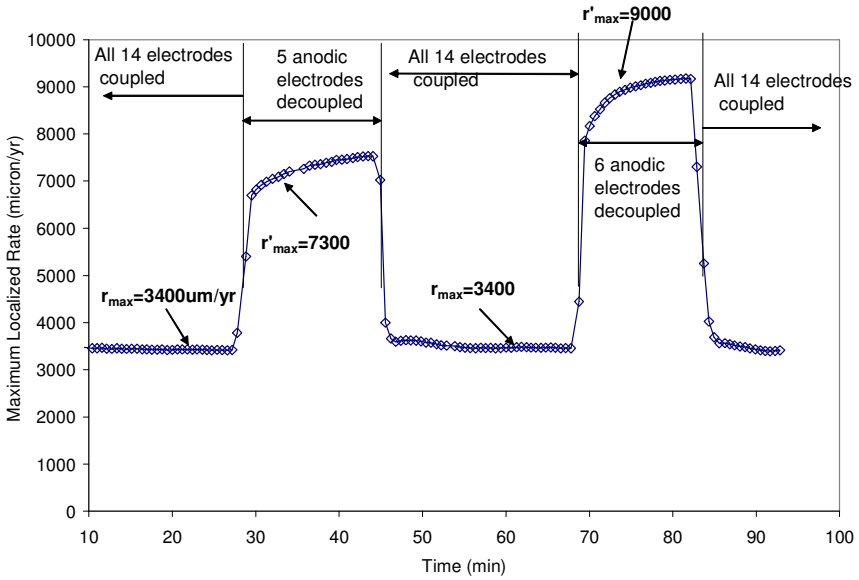

FIGURE 9. Comparison between the localized corrosion rate obtained from the most corroding electrode without decoupling the less anodic electrode and the localized corrosion rate obtained from the most corroding electrode with decoupling the less anodic electrodes.

Patent pending.